JACS
JOURNAL OF THE AMERICAN CHEMICAL SOCIETY
Article
pubs.acs.org/JACS

Spectroelectrochemical Signatures of Capacitive Charging and Ion Insertion in Doped Anatase Titania Nanocrystals

Clayton J. Dahlman,[†] Yizheng Tan,[†,‡] Matthew A. Marcus,[§] and Delia J. Milliron*[,†]

[†]McKetta Department of Chemical Engineering, The University of Texas at Austin, 200 E. Dean Keeton Street, Austin, Texas 78712, United States

[‡]The Molecular Foundry and [§]The Advanced Light Source, Lawrence Berkeley National Laboratory, 1 Cyclotron Rd., Berkeley, California 94720, United States

Supporting Information

ABSTRACT: Solution-processed films of colloidal aliovalent niobium-doped anatase TiO_2 nanocrystals exhibit modulation of optical transmittance in two spectral regions—near-infrared (NIR) and visible light—as they undergo progressive and reversible charging in an electrochemical cell. The Nb-TiO_2 nanocrystal film supports a localized surface plasmon resonance in the NIR, which can be dynamically modulated via capacitive charging. When the nanocrystals are charged by insertion of lithium ions, inducing a well-known structural phase transition of the anatase lattice, strong modulation of visible transmittance is observed. Based on X-ray absorption near-edge spectroscopy, the conduction electrons localize only upon lithium ion insertion, thus rationalizing the two modes of optical switching observed in a single material. These multimodal electrochromic properties show promise for application in dynamic optical filters or smart windows.

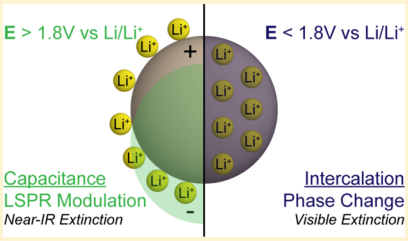

INTRODUCTION

Electrochromic materials, which change color, transparency, and reflectivity upon the application of an external potential, can have significant impact on energy consumption as films in architectural smart windows.[1] In particular, precise independent spectral control over material transmittance in the visible and near-infrared (NIR) regimes of the solar spectrum is necessary to develop next-generation electrochromic smart windows for improved energy efficiency in buildings. Amorphous transition-metal oxides, especially WO_3, have been the most studied materials for electrochromic windows; they exhibit optical modulation primarily in the visible range due to localized excitations of reduced metal cations.[2] Some metal oxide semiconductors, when synthesized instead as colloidal nanocrystals (NCs), are capable of supporting tunable localized surface plasmon resonance (LSPR) that interacts with NIR light, forming the basis for spectrally complementary electrochromic modulation.[3]

We hypothesized that in doped transition-metal oxide NCs, the visible-band optical modulation due to the traditional cation intercalation process could coexist with the NIR LSPR extinction. This NIR effect has been previously shown to be tunable by synthetic doping[3] and can be modulated postsynthetically by electrochemical charging in the case of Sn-doped indium oxide (ITO)[4] and aluminum-doped zinc oxide (AZO) NCs.[5] Thus, NCs of synthetically doped transition-metal oxides should be capable of independent modulation in two spectral bands (visible and NIR) within a single-component functional film. Here, we demonstrate such dual-mode modulation in anatase TiO_2 doped with niobium.

Anatase TiO_2 is a well-known lithium insertion material that has been studied as a battery electrode.[6−10] Attempts to improve the slow lithium diffusion kinetics and conductivity of bulk anatase have yielded nanostructured TiO_2 electrodes that demonstrate significant improvements in charge capacity and charging rates.[8−15] Surface charging has been hypothesized to account for nearly as much charge capacity as the lithium insertion reaction in TiO_2 once particle sizes approach 10 nm.[12] Along with nanostructuring, the electrochemical behavior of TiO_2 electrodes has been improved by aliovalent doping with niobium or tantalum to increase the inherently low conductivity of TiO_2.[15−19] At diameters around 10 nm, degenerately doped NCs can support LSPR, which can be tuned across the infrared and visible spectrum by varying the NC size, shape, composition and Fermi level, as seen in ITO, AZO, and other semiconductor colloidal NCs.[3,20] Niobium-doped anatase TiO_2 (Nb-TiO_2) exhibits a broad mid-IR LSPR extinction peak when synthesized as 10 nm diameter colloidal NCs, which can be tuned in amplitude and energy by varying the amount of Nb doping.[21] Anatase TiO_2 is also known to be electrochromic; intercalation of Li^+ produces a visible extinction feature at about 730 nm.[22] This peak has been ascribed to localization of injected electrons on Ti cations,[23] creating a polaronic lattice distortion,[24,25] which is similar to the proposed mechanisms for electrochromism in amorphous transition-metal oxides, such as WO_3 and NbO_x[2].

Received: May 12, 2015
Published: July 8, 2015

DOI: 10.1021/jacs.5b04933
J. Am. Chem. Soc. 2015, 137, 9160−9166

EXPERIMENTAL SECTION

Nb-TiO_2 NCs were synthesized by a slightly modified literature procedure.[21] Nb doping content in this study is expressed as the percentage of Ti sites occupied by Nb in the anatase structure, as measured by inductively coupled plasma-optical emission spectroscopy. The Nb:Ti ratio in the feedstock was found to be roughly equal to the substitutionally doped NC cation ratio up to about 10% Nb substitutional content. Excess Nb precursor was required to dope beyond 10%, and it was difficult to achieve doping concentrations above 20%.

Conductive mesoporous films of colloidal TiO_2 NCs were prepared by spin-coating solutions of ligand-stripped NCs and annealing. The oleic acid ligands bound to the surface of the colloidal NCs upon synthesis were stripped in solution using nitrosonium tetrafluoroborate ($NOBF_4$), following literature procedures.[26] The ligand-stripped particles in a solution of acetonitrile and *N*,*N*-dimethylformamide (4:1 by volume) were spin-cast on either ITO-coated glass or silicon wafers. Uniform films of 100−200 nm were confirmed by profilometry. The films were annealed under argon at 300 °C for 30 min to remove residual organics.

For electrochemical testing, the NC-coated substrate was used as the working electrode, and a single strip of lithium metal was used as both the counter and reference electrode, under an argon atmosphere. Transmission spectra were recorded *in situ* during cycling using a fiber-coupled spectrometer. Strong absorption bands from the liquid electrolyte limited the spectral window to 400−2200 nm for these *in situ* experiments.

Ex situ X-ray diffraction (XRD) of electrochemically charged NC films was performed at the Stanford Synchrotron Radiation Laboratory (SSRL) at beamline 11-3. Diffraction patterns were obtained in transmission and, for some data in the Supporting Information, grazing-incidence. Substrates of p-type (boron-doped) silicon wafers were used for transmission experiments. NC films were electrochemically charged as described above, then rinsed with dimethyl carbonate to prevent deposition of salts from the electrolyte. The charged films were sealed air-free in a Kapton pouch; single-crystal silicon peaks were subtracted out using baseline patterns from an uncoated portion of the sample substrate.

Ex situ X-ray absorption spectra were collected at the Advanced Light Source (ALS) at beamline 10.3.2 by detection of X-ray fluorescence. Films of electrochemically charged ligand-stripped NCs were prepared as described above for synchrotron XRD. The charged films were mounted on an aluminum sample holder and sealed with a thin Mylar film.

Ex situ mid-IR extinction measurements of the charged NC films were obtained using a Fourier transform infrared (FTIR) spectrometer. Undoped silicon substrates were coated with 3 nm of chromium followed by 10 nm of gold to provide a conductive but semi-transparent substrate. Ligand-stripped NC films around 500 nm thick were coated by spin coating, then charged and rinsed, as described above. The charged films were assembled air-free into an O-ring sealed cell with a CaF_2 window for measurement in transmission mode.

DISCUSSION

The synthesized NCs are 11 nm cuboids for doping levels up to about 10% Nb, above which they become slightly larger, more polydisperse and anisotropic, consistent with previously published results (Figure 1a,b).[21] Spin-coated films are optically clear and free of gross defects (Figure 1c).

We charged and discharged films of ligand-stripped NCs in galvanostatic mode to test the impact of Nb doping on electrochemical behavior. A lithium-based liquid electrolyte, 0.1 M bis(trifluoromethane)sulfonimide lithium (LiTFSI) in tetraglyme, was used. The voltage profiles (Figure 2), normalized by empirical discharge capacity at a rate of 1C for each sample, demonstrate three distinct electrochemical regions. A charging plateau is centered near 1.8 V vs Li/Li^+

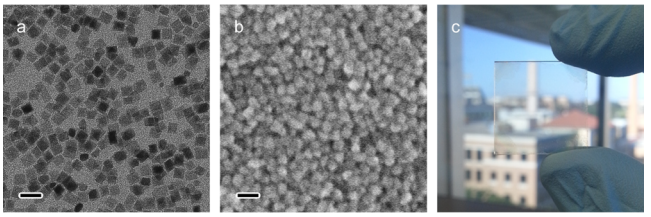

Figure 1. (a) Low-resolution TEM image of 2% Nb-doped TiO_2 NCs. The scale bar is 20 nm. (b) Top-down SEM of a spin-coated film of 5% Nb-TiO_2 NCs. The scale bar is 20 nm. (c) Photograph of a 2 cm square ITO-coated glass substrate coated by a 180 nm thick film of 5% Nb-TiO_2 NCs.

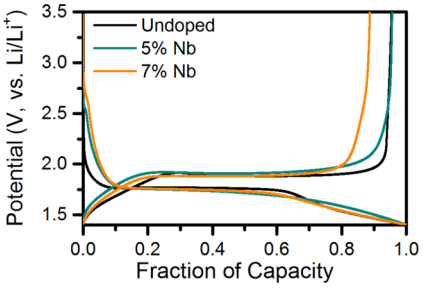

Figure 2. Galvanostatic charging profiles for films of Nb-TiO_2 NCs at an approximate rate of 1C. The electrolyte was 0.1 M LiTFSI in tetraglyme.

with a 0.15 V overpotential difference between the charge and discharge curves for the entire range of Nb doping (see Figure S1 for expanded doping range). At potentials above and below the plateau, there is significant charging approaching both potential limits of the experiment. These observations are consistent with previous studies of anatase TiO_2 NCs, which attribute the charging plateau to a two-phase region where Li^+ intercalates into the anatase crystal lattice, leading to a distorted orthorhombic $Li_{0.5}TiO_2$ phase.[13,27−30]

$$TiO_2 + xLi^+ + xe^- \rightleftharpoons Li_xTiO_2; \quad x < 0.5$$

The behavior at potentials above and below the constant-voltage plateau is actively debated; capacitive charging is commonly described as a dominant process, especially for potentials below the plateau, and solid-solution intercalation of lithium in anatase is found to account for stoichiometries up to $Li_{0.2}TiO_2$ for potentials above 1.8 V. The relative contributions of solid-solution intercalation and capacitive charging, particularly for potentials above 1.8 V, is actively studied for nanocrystalline TiO_2.[10−14] The constant-voltage plateau for Nb-TiO_2 NCs accounts for about half of the charge capacity of our films, consistent with previous results for 10 nm (undoped) anatase TiO_2 NCs.[12] The consistency of the galvanostatic curves across doping levels reveals that Nb doping only has a minor effect on the electrochemical lithiation and delithiation of anatase TiO_2 NC thin films.

The crystal structure of Nb-TiO_2 NCs was studied *ex situ* by XRD to assess the impact of Nb incorporation on the intercalation phase transition. The intercalation of lithium into bulk anatase TiO_2 induces a phase transition to orthorhombic $Li_{0.5}TiO_2$, observable by XRD.[11,31] Our NC films were evaluated at three points in the discharge curve: 4 V (fully oxidized), 1.8 V (reduced almost to the constant-voltage plateau), and 1.5 V (fully reduced). Comparing our results to reference patterns for anatase TiO_2 and $Li_{0.5}TiO_2$,[28] we see that

DOI: 10.1021/jacs.5b04933
J. Am. Chem. Soc. 2015, 137, 9160−9166

the NCs transition from tetragonal anatase to orthorhombic $Li_{0.5}TiO_2$ upon crossing the constant-voltage plateau (Figure 3). The phase change reverses under oxidation, but there is

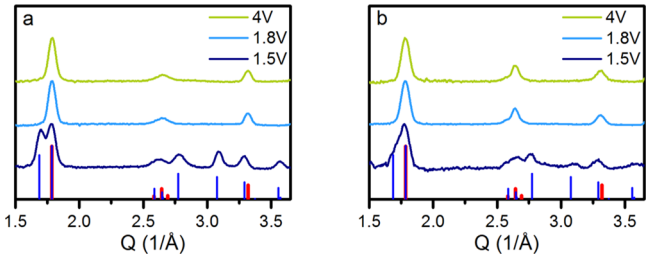

Figure 3. Transmission wide-angle XRD of electrochemically charged (a) undoped and (b) 10% Nb-doped NC films. The as-deposited and partially reduced 1.8 V patterns match the anatase structure ($I4_1/amd$, ICSD Coll. code 96946, red), and the fully reduced 1.5 V pattern corresponds to the $Li_{0.5}TiO_2$ phase (*Imma*, ICSD Coll. code 96948, blue), reported for microscale anatase TiO_2.[28]

some evidence for phase mixing (i.e., early, partial conversion to the anatase phase) at potentials below the 1.9 V phase coexistence plateau (Figures S3 and S4). The reversible phase behavior and general electrochemical characteristics of anatase TiO_2 NCs are maintained over a wide range of Nb doping levels (see additional XRD data, Figure S4). In all cases, two distinct electrochemical charging processes occur: a crystalline phase change accompanies faradaic lithium intercalation, and a rapid charging process occurs within the anatase TiO_2 phase. These two electrochemical processes can be anticipated to yield distinct optical signatures.

Initially, Nb-TiO_2 NC films are highly transparent in the visible region and exhibit a rising extinction feature in the NIR; this NIR extinction is enhanced upon electrochemical reduction or increased Nb doping. Indeed, undoped TiO_2 NCs, initially transparent across the visible and NIR, begin to absorb in the NIR as they are charged (Figure 4). The change in NIR optical

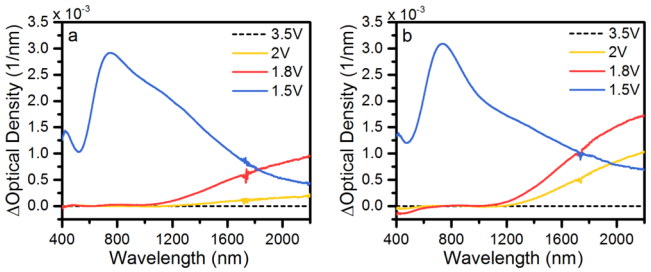

Figure 4. *In situ* spectroelectrochemistry of (a) undoped and (b) 5% Nb-doped TiO_2 NC films. Spectra are reported as ΔOptical Density referenced to the as-deposited films and normalized by film thickness to account for minor sample-to-sample differences. The electrolyte was 0.1 M LiTFSI in tetraglyme.

density with applied voltage varies with Nb doping level, reaching a maximum modulation around 7% Nb (Figure S7). At reducing potentials beyond the phase-change threshold, a visible extinction peak arises around 730 nm, observable for all levels of Nb doping. Previous studies have reported similar visible-range electrochromism of TiO_2 NCs reduced in Li^+-containing electrolytes.[22,24,32] However, the spectral range in those studies was limited, and no significant IR modulation was observed.

The NIR transmittance modulation we observe in both undoped and Nb-TiO_2 NCs (Figure 4) suggests that electrons injected prior to the two-phase potential plateau populate delocalized conduction band states rather than self-trapping and localizing in polaronic states. The Fermi level of anatase lies within the bandgap, and the conduction band is derived primarily from Ti 3d orbitals.[33,34] Electron accumulation, by electrochemical charging, doping or other means, can either populate these conduction band states, generate polaronic states by self-trapping, or interact with Ti or O defects.[35−37] The literature is conflicted on which of these processes are dominant.[25] Recent computational studies have explained the metallic conductivity of Nb-TiO_2 with a theory that describes substitutional Nb defects as shallow electron donors,[35,38] but electrons accumulated by capacitive charging are still poorly understood. Our results suggest that capacitive electron accumulation, like Nb doping, enhances NIR LSPR extinction. Earlier studies have reported blue shifts of NIR extinction peaks and increased NIR extinction in doped metal oxide NCs under electrochemical or chemical charging and have successfully modeled these phenomena as changes to LSPR extinction upon increasing free electron concentration.[3,39]

On the other hand, the visible electrochromic effect in orthorhombic $Li_{0.5}TiO_2$ is theorized to be due to polaronic reduced Ti^{3+} states,[24,25] so we hypothesized that delocalized and localized excess electrons may be present at different stages of the charging process. *Ex situ* X-ray absorption near-edge spectroscopy (XANES) was used to assess the influence of Nb on polaronic charge trapping behavior of excess electrons in TiO_2 both before and as a result of electrochemical cycling. The pre-edge structure of the Ti K-edge is diagnostic of the effective oxidation state and was examined for evidence of changes in the oxidation state of Ti atoms upon doping or electrochemical charging (Figures 5 and 6).

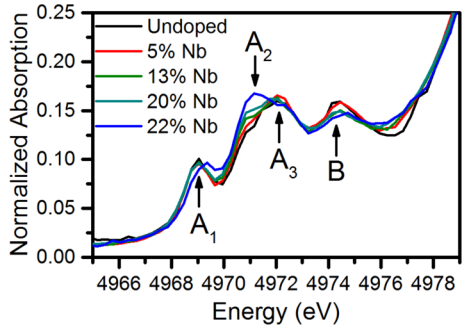

Figure 5. XANES Ti pre-K edge spectra for uncharged films of varying Nb doping content.

The effects of Nb doping on electron correlation in uncharged anatase TiO_2 are an active area of debate. Several studies have found evidence of electron correlation in Nb-TiO_2 from XPS[40−42] and EPR measurements,[43] leading to observed Ti^{3+} sites, but de Trizio et al.'s recent studies of colloidal Nb-TiO_2 NCs found no evidence of electron correlation at room temperature using XPS or EPR.[21] The latter technique revealed localization only below about 100 K. We obtained XANES spectra of the Ti K-edge for a broad range of Nb doping (Figure 5). The Ti K-edge position, measured by the maximum of the absorption first derivative, shows no discernible shift upon any level of Nb doping (Figure S5). Thus, we can confirm that Nb doping does not have a major impact on the formal

DOI: 10.1021/jacs.5b04933
J. Am. Chem. Soc. 2015, 137, 9160−9166

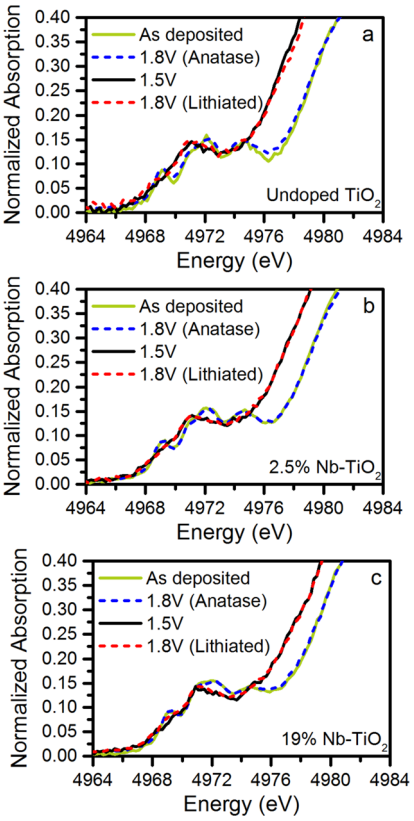

Figure 6. Titanium XANES pre-K edge spectra upon *ex situ* charging, of (a) undoped, (b) 2.5% Nb-doped, and (c) 19% Nb-doped TiO_2 NCs.

valence of Ti in these Nb-TiO_2 NCs. Oxygen stoichiometry may play a significant role in the conflict between these results and earlier studies, because the processing conditions for Nb-TiO_2 NCs used in this study, at atmospheric pressure and relatively low temperatures (below 300 °C), deviate from many earlier studies.[37] Although doped Nb does not change the formal valency of Ti, it does induce systematic changes in the pre-edge features at high doping concentrations. Using the lettering system common in the literature, A_1, A_2, A_3 for Ti 1s to 3d transitions and B for Ti 1s to 4p transitions,[44−46] we can see that beyond 20% Nb, the A_2 peak notably increases in relative intensity, along with shifts in the other peak energies and amplitudes (Figure 5). Similar effects have been attributed to symmetry breaking in the anatase lattice due to defects or strain, suggesting that high levels of doped Nb may affect the local structure of anatase TiO_2.[47,48] Nb doping has been shown to expand the anatase lattice,[15,16] and Nb appears to surface segregate in Nb-TiO_2 NCs at high doping concentrations,[21] so it is reasonable to expect strain associated with Nb defects to distort the symmetry of local TiO_6 octahedra.

The phase change from anatase to $Li_{0.5}TiO_2$ has been shown to correlate to a reduction in the average charge state of Ti cations in anatase.[45,46] Indeed, our XANES data mirror the phase behavior we observed by XRD: For potentials above the intercalation threshold, the Ti K-edge remains at a higher energy, as expected for Ti^{4+} in anatase TiO_2.[46] (Figure 6). After the orthorhombic phase change the Ti K-edge energy decreases by 2 ± 0.3 eV. Both Wagemaker et al.[45] and Lafont et al.[46] report an edge shift around 1.5 eV upon lithiation to $Ti^{3.5+}$ ($Li_{0.5}TiO_2$), for microscale and nanocrystalline anatase TiO_2, respectively. The edge shift we observe (Figure 6), suggests that Ti cations in Nb-TiO_2 NCs are reduced to an average valence of roughly $Ti^{3.5+}$ upon lithiation to the orthorhombic phase, consistent with one-half Li^+ per formula unit. However, Ti valency does not change upon charging at potentials above or below the two-phase potential plateau, conflicting with previous reports of a solid solution of Li and anatase TiO_2 in these potential regions.[10−12,46] Likewise, we find no evidence from spectroelectrochemistry (Figure 4) to support the localization of electrons at titanium bulk or surface sites at potentials above the orthorhombic phase-transition threshold. Rather, the results suggest that only $Li_{0.5}TiO_2$ demonstrates charge localization and that capacitive charging dominates above and below the two-phase potential with the accumulated charge occupying delocalized states where it enhances NIR LSPR extinction. Lithium insertion—coupled to the orthorhombic phase transition—drives charge localization, causing the appearance of a polaronic, visible extinction peak. Considering all the XANES results (Figures 5 and 6), we conclude that electrons in Nb-TiO_2 NCs are delocalized, as are electrons added during capacitive charging at potentials above and below the two-phase potential. Only upon lithiation do electrons localize at Ti cation sites.

Our XANES results indicate that capacitive charging populates delocalized conduction band states and that lithium insertion is required to induce localization. Thus, we predicted no visible electrochromism would occur in the absence of a small cation, such as Li^+. Rather, we anticipate that only NIR LSPR modulation should be possible if a bulky, nonintercalating cation, such as tetrabutylammonium (TBA^+) is employed in the electrolyte. To test this hypothesis, the electrochromic response was measured by *in situ* spectroelectrochemistry using a non-intercalating 0.1 M tetrabutylammonium-TFSI in tetraglyme electrolyte. The same film measured with Li-TFSI (Figure 4) was electrochemically cycled in the TBA^+ electrolyte, using a single silver wire as a counter and reference electrode. The potentials reported in Figure 7 are referenced to

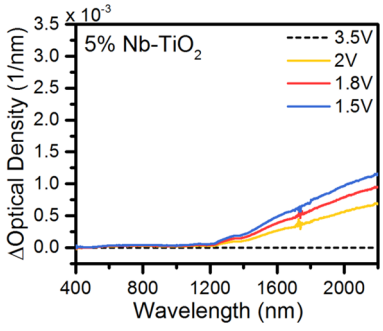

Figure 7. *In situ* spectroelectrochemistry of 5% Nb-doped TiO_2 NC film. The spectrum is reported as ΔOptical Density referenced to the as-deposited film extinction and normalized by film thickness. The electrolyte was 0.1 M TBA-TFSI in tetraglyme.

Li/Li^+, based on a conversion from the Ag/Ag^+ reference used in the experiment. The film darkens in the NIR (Figure 7), however, charging in TBA^+ electrolyte does not induce a visible extinction at any potential, consistent with earlier results for undoped TiO_2,[22] and reducing potentials beyond the lithiation threshold only increase the extent of NIR modulation. The TBA^+ ion is too large to intercalate into the anatase lattice, so we can confirm that capacitive electrochemical charging—

DOI: 10.1021/jacs.5b04933
J. Am. Chem. Soc. 2015, 137, 9160−9166

whether in Li^+ or TBA^+ electrolyte—populates delocalized conduction band states, giving rise to increased NIR extinction.

Furthermore, the continuous increase of a NIR extinction with applied bias is qualitatively consistent with the electrochromic behavior previously observed in plasmonic metal oxide NCs (ITO and AZO).[4,39] The mid-IR electrochromic response of Nb-TiO_2 NCs was measured *ex situ* to observe the full optical response of the LSPR peak profile to capacitive charging (Figure 8). The films were charged in a Li-ion-containing

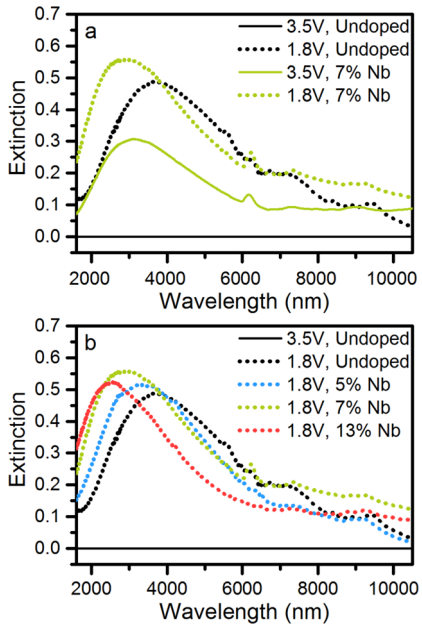

Figure 8. Transmission FTIR spectra of *ex situ* charged NC films. Spectra were referenced to the oxidized (3.5 V) undoped TiO_2 film and normalized by thickness. (a) Comparison of oxidized (3.5 V) and capacitively charged (1.8 V) films for a range of Nb doping content. (b) Comparison of the capacitively charged (1.8 V) films for various doping levels.

electrolyte, but the potential was restricted to remain in the capacitive charging regime, avoiding the orthorhombic phase transition. Nb doping clearly increases MIR extinction of uncharged TiO_2 NC films, leading to well-defined peaks that are consistent with results ascribed to LSPR extinction in the previous study of Nb-TiO_2 NCs[21] (Figure 8a). Upon capacitive reduction, MIR extinction increases for all Nb doping levels (Figures 8a and S8), and the peak wavelength decreases with increasing doping (Figure 8b).

Electrochromic effects in the visible and NIR bands occur by independent electrochemical charging processes: lithium intercalation leads to electron localization at Ti sites for the former, while population of conduction band states during capacitive charging leads to LSPR modulation for the latter. The independence of these two electrochromic modes can be exploited further by modulating electrochemical capacitive charge of the lithium intercalated phase ($\sim Li_{0.5}TiO_2$). At reducing potentials negative of the intercalation threshold, lithiated TiO_2 NCs accumulate charge by capacitance as demonstrated in the XANES and XRD results, leading to a modulation in the near-IR extinction of the $Li_{0.5}TiO_2$ phase as shown in Figure 9. The fully reduced film at 1.5 V shows a maximum visible extinction and moderate NIR extinction, but upon reoxidation to 1.8 V, the visible peak is retained, while NIR extinction decreases significantly. This effect is consistent with free electron depletion upon capacitive oxidation, leading to a decrease in extinction of an LSPR peak. The independent switching of visible and NIR electrochromic modes in a single component inorganic material is unprecedented and holds the tantalizing promise that rich, multifunctional optical control devices can be achieved using simple processing strategies for a single-component NC film.

CONCLUSIONS

Two modes of electrochromism—plasmonic and polaronic—coexist in one material, Nb-TiO_2 NCs. Capacitive charging of TiO_2 NCs induces infrared extinction, which is tunable by doping. In this state, the charge carriers remain delocalized. This "cool" infrared-blocking mode is well established for previous studies of plasmonic metal oxide NCs[3] but has not been well explored in TiO_2. In fact, even the delocalization of electrons in doped TiO_2 (e.g., Nb-TiO_2) is actively debated, but that theory is strongly supported by our Ti K-edge XANES spectra. The electrons persist in delocalized states throughout the capacitive charging process. Only upon insertion of Li^+ ions, and transition to the orthorhombic $Li_{0.5}TiO_2$ phase, do the electrons localize, forming Ti^{3+} polaronic color centers with a

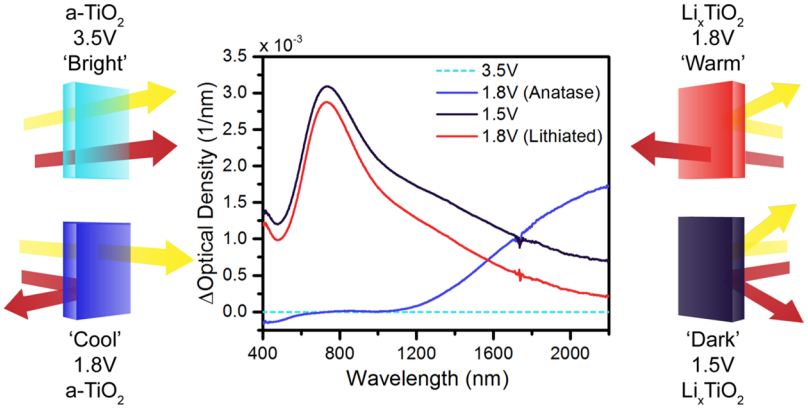

Figure 9. *In situ* spectroelectrochemistry of 5% Nb-doped TiO_2 NC films showing four distinct electrochromic states with different transmittance of visible (yellow arrow) and infrared (red arrow) light. Spectra are reported as ΔOptical Density referenced to the as-deposited film extinction and normalized by film thickness. The electrolyte was 0.1 M LiTFSI in tetraglyme. The "cool" mode is accessed by reducing from the "bright" mode, while the "warm" mode is accessed by oxidizing from the "dark" mode.

DOI: 10.1021/jacs.5b04933
J. Am. Chem. Soc. 2015, 137, 9160–9166

characteristic visible extinction. The lithiated phase ("dark" mode) blocks infrared and visible light, but infrared extinction can be diminished by capacitive oxidation (a "warm" mode). This kind of dual band modulation has long been a goal of electrochromics research and was only recently demonstrated by combining plasmonic metal oxide NCs with an amorphous transition-metal oxide, forming a composite of two single band electrochromic materials.[49] Our study demonstrates how dual mode electrochromic behavior can be achieved with a single-component solution-processed inorganic film.

More broadly, our results shed light on the nature of charge carriers in anatase TiO_2. We have presented broad evidence that plasmonic and polaronic excitation processes occur by discrete charging pathways. The interaction between conductivity, charging behavior, and structure has implications on the performance of TiO_2 as an electrode material. Likewise, photocatalytic and photovoltaic applications of TiO_2 are also impacted by charge-transport efficacy and stability issues, which can be mitigated by a careful understanding of surface and bulk charge localization in TiO_2.[50−54] The intersection of independent light-matter interactions—LSPR extinction and localized color centers—in colloidal TiO_2 NCs provides a novel means to decouple different optoelectronic processes in this important material.

■ ASSOCIATED CONTENT

Supporting Information

Details of nanocrystal synthesis, film deposition, scanning electron microscopy (SEM) and transmission electron microscopy (TEM), electrochemical and optical characterization techniques, additional XRD results and discussion of structural transformations, and additional optical trends with Nb-doping content. The Supporting Information is available free of charge on the ACS Publications website at DOI: 10.1021/jacs.5b04933.

■ AUTHOR INFORMATION

Corresponding Author

*milliron@che.utexas.edu

Notes

The authors declare the following competing financial interest(s): D.J.M. declares a financial interest in Heliotrope Technologies, a company pursuing commercial development of electrochromic windows.

■ ACKNOWLEDGMENTS

The authors thank Dr. Luca de Trizio for synthesis of Nb-TiO_2 NCs used in preliminary studies and Dr. Guillermo Garcia for exploratory spectroelectrochemical measurements of Nb-TiO_2 NCs. This research was supported by a U.S. Department of Energy (DOE) ARPA-E grant. D.J.M. acknowledges support of the Welch Foundation (F-1848). Some of this research was carried out at the Molecular Foundry, Lawrence Berkeley National Laboratory, a user facility supported by the Office of Science, Office of Basic Energy Sciences, of the U.S. Department of Energy under contract no. DE-AC02-05CH11231. Use of SSRL, SLAC National Accelerator Laboratory, is supported by DOE under contract no. DE-AC02-76SF00515. C.J.D. was supported by a National Science Foundation Graduate Research Fellowship under grant no. DGE 1106400.

■ REFERENCES

(1) Gillaspie, D. T.; Tenent, R. C.; Dillon, A. C. *J. Mater. Chem.* **2010**, *20*, 9585.
(2) Granqvist, C. G. *Sol. Energy Mater. Sol. Cells* **2012**, *99*, 1.
(3) Runnerstrom, E. L.; Llordes, A.; Lounis, S. D.; Milliron, D. J. *Chem. Commun.* **2014**, *50*, 10555.
(4) Garcia, G.; Buonsanti, R.; Runnerstrom, E. L.; Mendelsberg, R. J.; Llordes, A.; Anders, A.; Richardson, T. J.; Milliron, D. J. *Nano Lett.* **2011**, *11*, 4415.
(5) Garcia, G.; Buonsanti, R.; Llordes, A.; Runnerstrom, E. L.; Bergerud, A.; Milliron, D. J. *Adv. Opt. Mater.* **2013**, *1*, 215.
(6) Ohzuku, T.; Takehara, Z.; Yoshizawa, S. *Electrochim. Acta* **1979**, *24*, 219.
(7) Huang, S. Y.; Kavan, L.; Exnar, I.; Grätzel, M. *J. Electrochem. Soc.* **1995**, *142*, L142.
(8) Kavan, L.; Grätzel, M.; Rathouský, J.; Zukal, A. *J. Electrochem. Soc.* **1996**, *143*, 394.
(9) Chen, J. S.; Tan, Y. L.; Li, C. M.; Cheah, Y. L.; Luan, D.; Madhavi, S.; Boey, F. Y. C.; Archer, L. A.; Lou, X. W. *J. Am. Chem. Soc.* **2010**, *132*, 6124.
(10) Shin, J.-Y.; Samuelis, D.; Maier, J. *Adv. Funct. Mater.* **2011**, *21*, 3464.
(11) Sudant, G.; Baudrin, E.; Larcher, D.; Tarascon, J.-M. *J. Mater. Chem.* **2005**, *15*, 1263.
(12) Wang, J.; Polleux, J.; Lim, J.; Dunn, B. *J. Phys. Chem. C* **2007**, *111*, 14925.
(13) Wagemaker, M.; Borghols, W. J. H.; Mulder, F. M. *J. Am. Chem. Soc.* **2007**, *129*, 4323.
(14) Kim, C.; Buonsanti, R.; Yaylian, R.; Milliron, D. J.; Cabana, J. *Adv. Energy Mater.* **2013**, *3*, 1286.
(15) Ghicov, A.; Yamamoto, M.; Schmuki, P. *Angew. Chem.* **2008**, *120*, 8052.
(16) Furubayashi, Y.; Hitosugi, T.; Yamamoto, Y.; Inaba, K.; Kinoda, G.; Hirose, Y.; Shimada, T.; Hasegawa, T. *Appl. Phys. Lett.* **2005**, *86*, 252101.
(17) Zhang, S. X.; Kundaliya, D. C.; Yu, W.; Dhar, S.; Young, S. Y.; Salamanca-Riba, L. G.; Ogale, S. B.; Vispute, R. D.; Venkatesan, T. *J. Appl. Phys.* **2007**, *102*, 013701.
(18) Hitosugi, T.; Furubayashi, Y.; Ueda, A.; Itabashi, K.; Inaba, K.; Hirose, Y.; Kinoda, G.; Yamamoto, Y.; Shimada, T.; Hasegawa, T. *Jpn. J. Appl. Phys.* **2005**, *44*, L1063.
(19) Osorio-Guillén, J.; Lany, S.; Zunger, A. *Phys. Rev. Lett.* **2008**, *100*, 036601.
(20) Ye, X.; Fei, J.; Diroll, B. T.; Paik, T.; Murray, C. B. *J. Am. Chem. Soc.* **2014**, *136*, 11680.
(21) De Trizio, L.; Buonsanti, R.; Schimpf, A. M.; Llordes, A.; Gamelin, D. R.; Simonutti, R.; Milliron, D. J. *Chem. Mater.* **2013**, *25*, 3383.
(22) Boschloo, G.; Fitzmaurice, D. *J. Phys. Chem. B* **1999**, *103*, 7860.
(23) Richter, J. H.; Henningsson, A.; Karlsson, P. G.; Andersson, M. P.; Uvdal, P.; Siegbahn, H.; Sandell, A. *Phys. Rev. B* **2005**, *71*, 235418.
(24) Morgan, B. J.; Watson, G. W. *Phys. Rev. B* **2010**, *82*, 144119.
(25) De Angelis, F.; Di Valentin, C.; Fantacci, S.; Vittadini, A.; Selloni, A. *Chem. Rev.* **2014**, *114*, 9708.
(26) Dong, A.; Ye, X.; Chen, J.; Kang, Y.; Gordon, T.; Kikkawa, J. M.; Murray, C. B. *J. Am. Chem. Soc.* **2011**, *133*, 998.
(27) Cava, R. J.; Murphy, D. W.; Zahurak, S.; Santoro, A.; Roth, R. S. *J. Solid State Chem.* **1984**, *53*, 64.
(28) Wagemaker, M.; Kearley, G. J.; van Well, A. A.; Mutka, H.; Mulder, F. M. *J. Am. Chem. Soc.* **2003**, *125*, 840.
(29) Morgan, B. J.; Watson, G. W. *J. Phys. Chem. Lett.* **2011**, *2*, 1657.
(30) Belak, A. A.; Wang, Y.; Van der Ven, A. *Chem. Mater.* **2012**, *24*, 2894.
(31) Wagemaker, M.; van de Krol, R.; Kentgens, A. P. M.; van Well, A. A.; Mulder, F. M. *J. Am. Chem. Soc.* **2001**, *123*, 11454.
(32) van de Krol, R.; Goossens, A.; Meulenkamp, E. A. *J. Appl. Phys.* **2001**, *90*, 2235.
(33) Asahi, R.; Taga, Y.; Mannstadt, W.; Freeman, A. J. *Phys. Rev. B* **2000**, *61*, 7459.

DOI: 10.1021/jacs.5b04933
J. Am. Chem. Soc. 2015, 137, 9160−9166

(34) Landmann, M.; Rauls, E.; Schmidt, W. G. *J. Phys.: Condens. Matter* **2012**, *24*, 195503.
(35) Lee, H. Y.; Robertson, J. *J. Appl. Phys.* **2013**, *113*, 213706.
(36) Shin, J.-Y.; Joo, J. H.; Samuelis, D.; Maier, J. *Chem. Mater.* **2012**, *24*, 543.
(37) Nogawa, H.; Hitosugi, T.; Chikamatsu, A.; Nakao, S.; Hirose, Y.; Shimada, T.; Kumigashira, H.; Oshima, M.; Hasegawa, T. *Jpn. J. Appl. Phys.* **2010**, *49*, 041102.
(38) Deák, P.; Aradi, B.; Frauenheim, T. *Phys. Rev. B* **2011**, *83*, 155207.
(39) Schimpf, A. M.; Lounis, S. D.; Runnerstrom, E. L.; Milliron, D. J.; Gamelin, D. R. *J. Am. Chem. Soc.* **2015**, *137*, 518.
(40) Hitosugi, T.; Kamisaka, H.; Yamashita, K.; Nogawa, H.; Furubayashi, Y.; Nakao, S.; Yamada, N.; Chikamatsu, A.; Kumigashira, H.; Oshima, M.; Hirose, Y.; Shimada, T.; Hasegawa, T. *Appl. Phys. Express* **2008**, *1*, 111203.
(41) Liu, Y.; Szeifert, J. M.; Feckl, J. M.; Mandlmeier, B.; Rathousky, J.; Hayden, O.; Fattakhova-Rohlfing, D.; Bein, T. *ACS Nano* **2010**, *4*, 5373.
(42) Bhachu, D. S.; Sathasivam, S.; Sankar, G.; Scanlon, D. O.; Cibin, G.; Carmalt, C. J.; Parkin, I. P.; Watson, G. W.; Bawaked, S. M.; Obaid, A. Y.; Al-Thabaiti, S.; Basahel, S. N. *Adv. Funct. Mater.* **2014**, *24*, 5075.
(43) Chiesa, M.; Paganini, M. C.; Livraghi, S.; Giamello, E. *Phys. Chem. Chem. Phys.* **2013**, *15*, 9435.
(44) Wu, Z. Y.; Ouvrard, G.; Gressier, P.; Natoli, C. R. *Phys. Rev. B* **1997**, *55*, 10382.
(45) Wagemaker, M.; Lützenkirchen-Hecht, D.; van Well, A. A.; Frahm, R. *J. Phys. Chem. B* **2004**, *108*, 12456.
(46) Lafont, U.; Carta, D.; Mountjoy, G.; Chadwick, A. V.; Kelder, E. M. *J. Phys. Chem. C* **2010**, *114*, 1372.
(47) Farges, F.; Brown, G. E. Jr.; Rehr, J. J. *Phys. Rev. B* **1997**, *56*, 1809.
(48) Angelome, P. C.; Andrini, L.; Calvo, M. E.; Requejo, F. G.; Bilmes, S. A.; Soler-Illia, G. J. A. A. *J. Phys. Chem. C* **2007**, *111*, 10886.
(49) Llordes, A.; Garcia, G.; Gazquez, J.; Milliron, D. J. *Nature* **2013**, *500*, 323.
(50) Hashimoto, K.; Irie, H.; Fujishima, A. *Jpn. J. Appl. Phys.* **2005**, *44*, 8269.
(51) Tong, H.; Ouyang, S.; Bi, Y.; Umezawa, N.; Oshikiri, M.; Ye, J. *Adv. Mater.* **2012**, *24*, 229.
(52) Bai, Y.; Mora-Sero, I.; De Angelis, F.; Bisquert, J.; Wang, P. *Chem. Rev.* **2014**, *114*, 10095.
(53) Ma, Y.; Wang, X.; Jia, Y.; Chen, X.; Han, H.; Li, C. *Chem. Rev.* **2014**, *114*, 9987.
(54) Schneider, J.; Matsuoka, M.; Takeuchi, M.; Zhang, J.; Horiuchi, Y.; Anpo, M.; Bahnemann, D. W. *Chem. Rev.* **2014**, *114*, 9919.

DOI: 10.1021/jacs.5b04933
J. Am. Chem. Soc. 2015, 137, 9160−9166